Electronic Supplementary Material (ESI) for Materials Chemistry Frontiers.

Supporting Information

Aromatic carbonyl compound-linked conjugated microporous polymer as an advanced cathode material for lithium-organic batteries

Kang Li[a,†], Qiang Li[a,†], Yunong Wang[a], Heng-guo Wang[a,b*], Yanhui Li[a], and Zhenjun Si[a,*]

[a] School of Materials Science and Engineering, Changchun University of Science and Technology, Changchun 130022, China.

[b] Key Laboratory of Polyoxometalate Science of the Ministry of Education and Faculty of Chemistry, Northeast Normal University, 5628 Renmin Street, Changchun, 130024, P. R. China.

[†] These authors contributed equally to this work and should be considered co-first authors.

*** Corresponding author.**

E-mail address: **wanghengguo@cust.edu.cn**; **szj@cust.edu.cn**

Experiment section

Materials.

Pyrene, 1,3,5-tris(4,4,5,5-tetramethyl-1,2-dioxaborolan-2-yl)benzene, sodium periodate ($NaIO_4$), tetrakis(triphenylphosphine)palladium(0), sodium bicarbonate ($NaHCO_3$), potassium carbonate (K_2CO_3), *N*-bromosuccinimide (NBS), trifluoroacetic acid (CF_3COOH) and 1-Methyl-2-pyrrolidinone (NMP) were purchased from Aladdin Chemical Reagent Co. Ltd. Ruthenium (III) chloride hydrate ($RuCl_3.xH_2O$) was purchased from J&K Scientific Co. Ltd. *N, N*-dimethylformamide (DMF, AR), dichloromethane (CH_2Cl_2, AR), dimethyl sulfoxide (DMSO, AR), acetonitrile (CH_3CN, AR), tetrahydrofuran (THF, AR), ethanol (AR) and methanol (AR) were purchased from Tianjin Fuyu Fine Chemical Co. Ltd. Sulfuric acid (H_2SO_4) was purchased from Beijing Chemicals Co. Ltd. All the materials were used without further purification. Water used in our experiments was deionized.

Synthesis of pyrene-4,5,9,10-tetraone (PT)

Pyrene-4,5,9,10-tetraone (PT) was synthesized according to the reported method.[S1,S2] In brief, pyrene (10 mmol, 2.02 g) was first dissolved in a mixture of 40 mL CH_2Cl_2 and 40 mL CH_3CN. Then, $NaIO_4$ (82 mmol, 17.5 g), 50 mL H_2O and $RuCl_3{\cdot}xH_2O$ (0.12 mmol, 0.25 g) were successively added to the mixture. The reaction mixture was stirred at 35-40 ^oC overnight. After reaction, the obtained mixture was poured into 500 mL deionized H_2O and then extracted by CH_2Cl_2, saturated $NaHCO_3$ solution and deionized H_2O, respectively. A dark yellow solid was obtained by condensing the organic solution, then, the crude product was recrystallized from DMSO to give 458 mg PT (17.5%, yield). 1H NMR (500 MHz, DMSO-d_6, ppm): 8.32 (d, 2H), 7.74 (t, 1H). FT-IR (KBr, cm^{-1}): 1673, 1561, 1443, 1341, 1281, 1054, 1030, 911, 821, 708. UV-Vis (DMF, nm): 267, 293, 373.

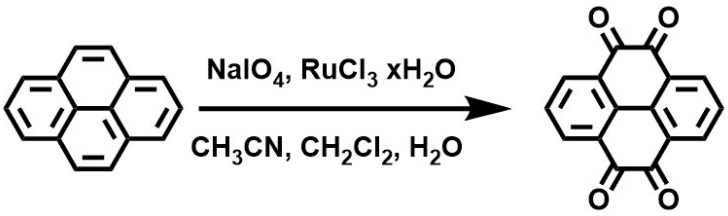

Scheme S1. Synthesize route of PT.

Synthesis of 2,7-dibromopyrene-4,5,9,10-tetraone (PT-2Br)

PT-2Br was synthesized according to the previous work.[S1,S3] Briefly, the recrystallized PT (1 mM, 262 mg) was dissolved in a mixture of 2 mL CF_3COOH and 5 mL H_2SO_4, then 1 mL H_2SO_4 solution with NBS (3 mM, 534 mg) was added into the obtained mixture drop by drop. Then, the mixture was kept at 40 ^oC for 2 days with stirring. After reaction, the product was poured into 20 mL H_2O and stirred for another 1 h. Finally, the crude product was collected by filtration and washed with saturated $NaHCO_3$ and H_2O until the filtrate reaches neutral. After recrystallized from DMSO, 240 mg yellow PT-2Br was obtained (58%, yield). 1H NMR (500 MHz, DMSO-d6, ppm): 8.36 (s). FT-IR (KBr, cm^{-1}): 1679, 1548, 1274, 1087, 1030, 900, 721. UV-Vis (DMF, nm): 271, 381.

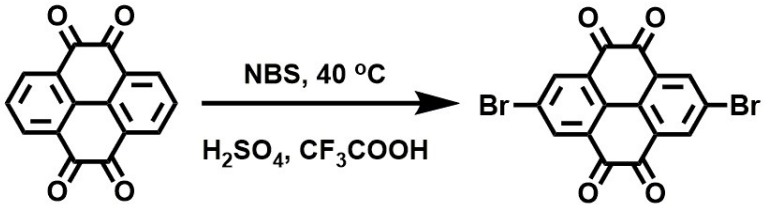

Scheme S2. Synthesize routes of PT-2Br.

Material Characterization.

Scanning electron micrograph (SEM) was performed by JEM-6701F (JEOL Ltd.). Powder X-ray diffraction (XRD) measurements were tested on Bruker D8 Focus Powder X-ray diffractometer using Cu Kα radiation (40 kV, 20 mA). Fourier transform infrared (FT-IR) spectra were determined by PerkinElmer Frontier

equipment using the KBr pellet technique and Raman spectra were collected with a Renishaw 2000 model confocal microscopy Raman spectrometer. ^{1}H NMR spectra were recorded in DMSO-d_6 on Bruker AV-500 (^{1}H 500 MHz). Thermal gravimetric (TG) analysis were carried out on TA SDT 2960 simultaneous thermal analyzer between 45 and 1000 ^{o}C at a heating rate of 10 ^{o}C min^{-1} under N_2.

Theory Calculation

All the calculations were performed with the Gaussian 09 package. The geometrical structures of the ground states were optimized at B3LYP/6-31 G(d) level in gas phase by the Density functional theory (DFT).[S4,S5] All calculated results of MESP were performed with Multiwfn 3.3.9 programs and the cubman utility provided by the Gaussian 09 program package.[S6] All visualization of MESP plots are carried out by Visual Molecule Dynamics (VMD) software.[S7]

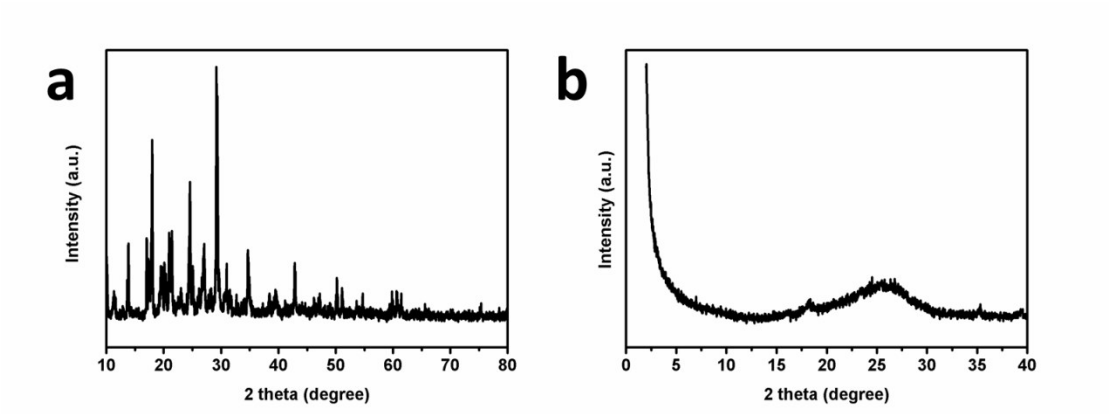

Figure S1. XRD spectra of PT and PT-BTA.

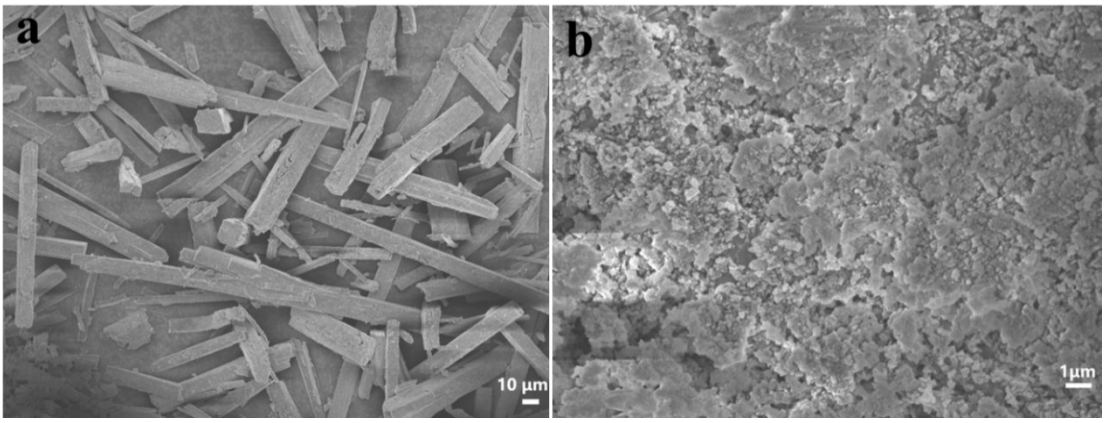

Figure S2. SEM images of (a) PT and (b) PT-BTA.

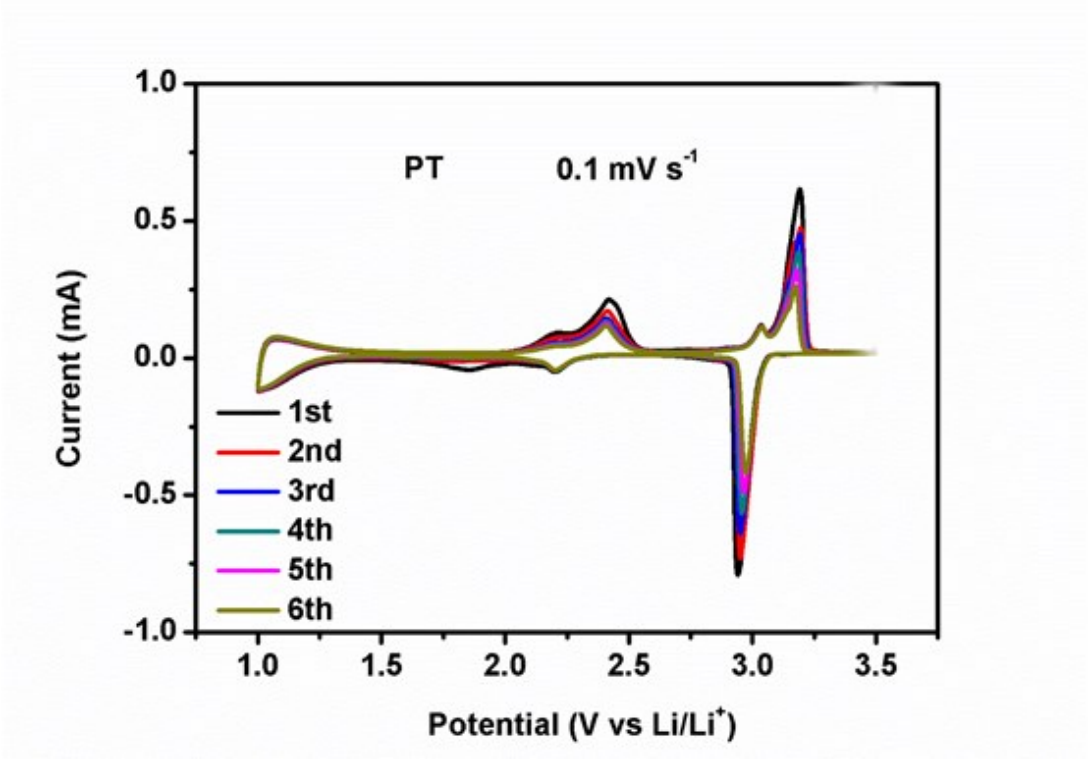

Figure S3. CV curves of PT at 0.1 mV s^{-1}.

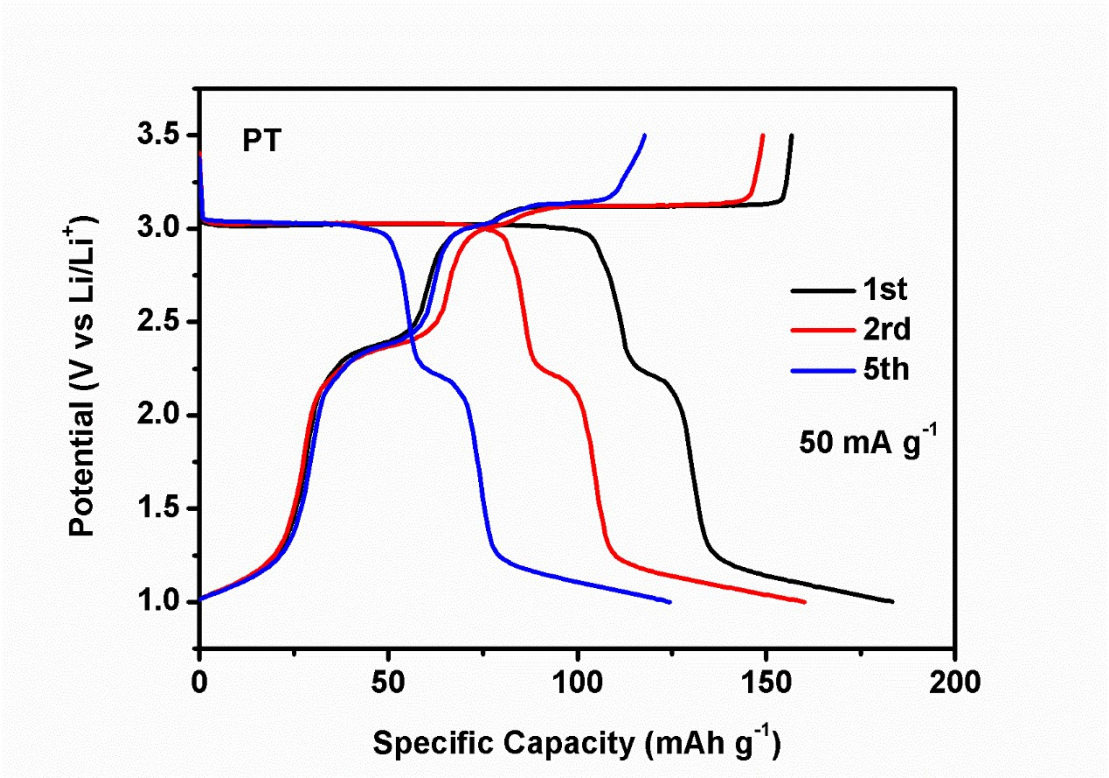

Figure S4. GDC profiles of PT at 0.05 A g^{-1}.

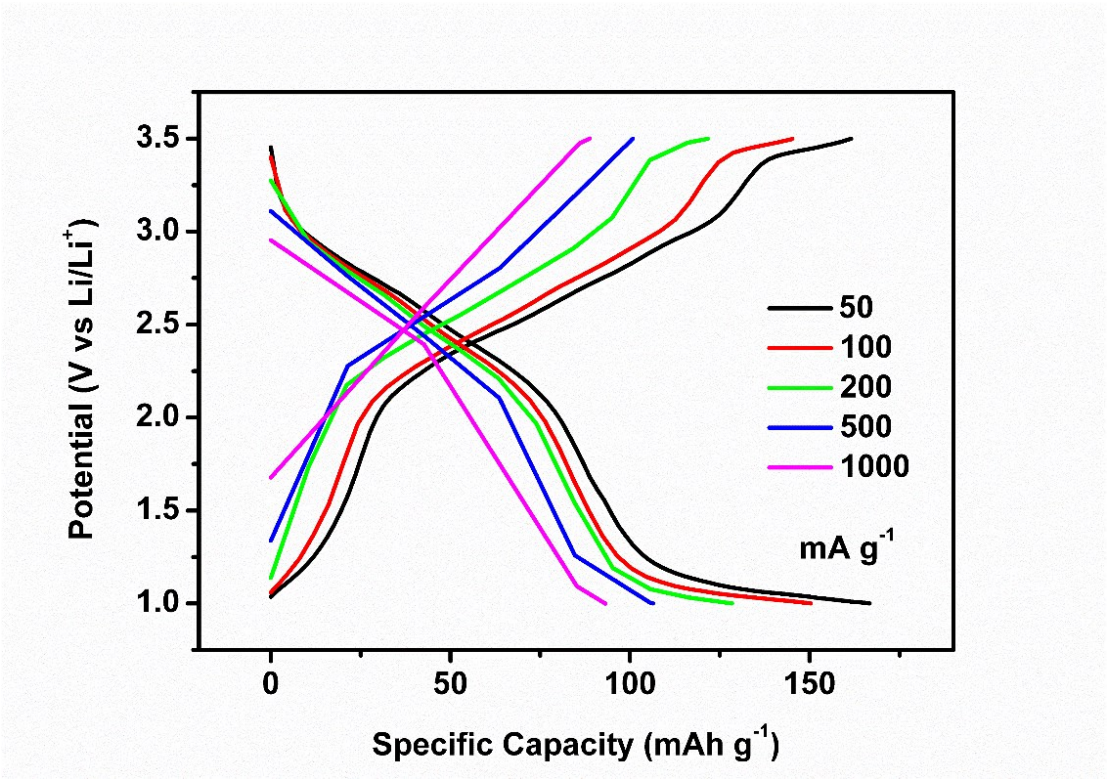

Figure S5. GDC profiles of PT-BTA at different current densities.

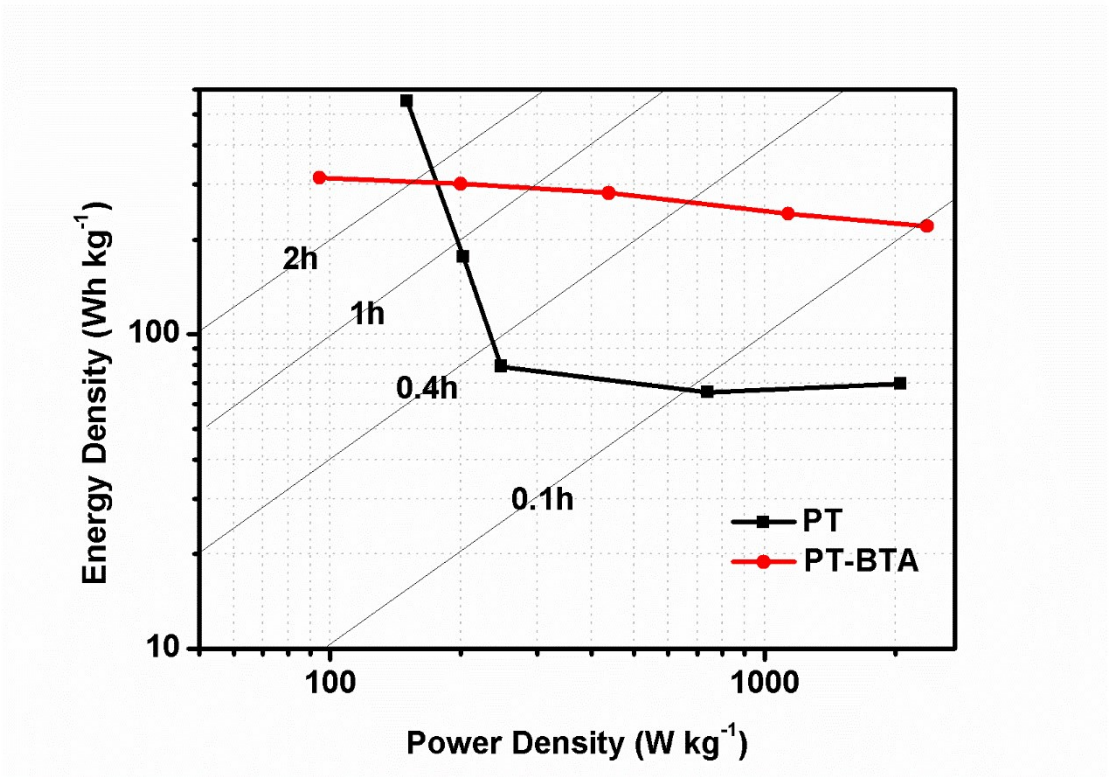

Figure S6. Ragone plots of PT and PT-BTA.

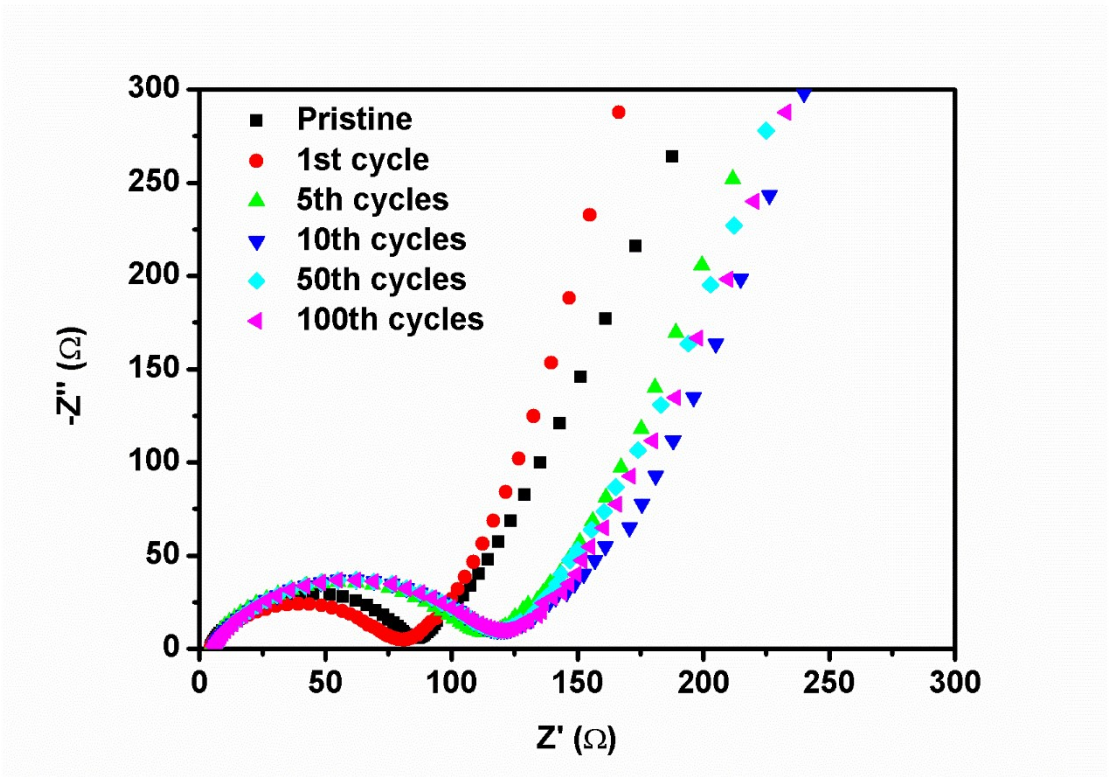

Figure S7. Nyquist plots of pristine PT-BTA cathode and after 1, 5, 10, 50 and 100 cycles.

Table S1. Summary of the electrochemical properties for organic electrode materials.

Electrode Materials	**Composition**	**Electrolytes**	**Discharge Voltage (V vs Li/Li$^+$)**	**Initial Discharge Capacity (mAh g^{-1})**	**Rate capacity (mA h g^{-1}) current density [mAg^{-1}/C]**
P(PyDI-T2)[S8]	Active: MWCNT =1:1	1M $LiPF_6$ in EC/DEC/DMC (v/v/v 1:1:1)	/	40.6	7.5/0.2C
NTAQ[S9]	Active: KB: PVDF= 6:3:1	1 M LiTFSI in DOL/DME (v/v 1:1)	2.25	130	62.4/5C
2D-PI@CNT[S10]	Active: SP: Alg-Na= 8:1:1	1 M LiTFSI in DOL/DME (v/v 1:1)	2.4	104.4	94/2A g^{-1}
IEP-11-E12[S11]	Active:MWCNT : PVDF= 5:4:1	1 M LiTFSI in DME/DOL (1:1 v/v)	2.2 V	104	23/5C
PPTC[S3]	Active: CNTs = 1:2	1 M LiTFSI in DOL/DME (v/v 1:1)	2.58	146.3	120.6/1 A g^{-1}
PTCDAS[S12]	Active: AB: PTFE= 80:15:5	1M $LiPF_6$ in EC/DMC (v/v1:1)	2.4	120-130	/
NOP[S13]	Active: KB: PVDF = 6:3:1	1M $LiPF_6$ in EC/DMC (v/v1:1)	2.52/2.48	175.4	133.5/0.5 A g^{-1}

NEP[S13]	Active: KB: PVDF= 6:3:1	1M $LiPF_6$ in EC/DMC (v/v1:1)	/	127.3	/
PI-1/2/3[S14]	Active: AB: PTFE= 80:15:5	1M $LiPF_6$ in EC/DEC/DMC (v/v/v 1:1:1)	/	61.7/103.4/ 78.1	/
S-PI[S15]	Active: SP: PVDF= 6:3:1	1M LiTFSI in DOL/DME (v/v 1:1)	2.5	150	/
PCFCs[S16]	Active: CNTs = 8: 10	1 M $LiPF_6$ in EC/DMC (v/v 1:1)	/	150	48/2 A g^{-1}
PGC40[S17]	Active: AB: PVDF= 8:1:1	1 M LiPF6 in EC/DMC (v/v 1:1)	/	152	86/1A g^{-1}
PT-BTA	Active: AB: PVDF= 3:6:1	1M LiTFSI in DOL/DME (v/v 1:1)	2.70/2.36	156.6	101.5/1A g^{-1} (3.16 C)

Table S2. MESP value of different atoms in PT-BTA calculated by DFT.

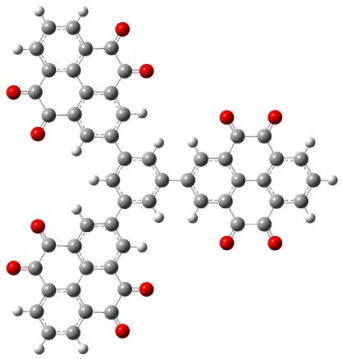

Molecular structure of PT-BTA

Atom	All	Positive	Negative	Atom	All	Positive	Negative
1	-17.82632	25.97811	-43.80443	20	31.89472	31.89472	NaN
2	-17.83244	25.97388	-43.80632	21	31.88199	31.88199	NaN
3	27.70868	27.70868	NaN	22	31.88948	31.88948	NaN
4	27.70819	27.70819	NaN	23	31.87400	31.87400	NaN
5	31.89305	31.89305	NaN	24	9.40428	9.40428	NaN
6	31.89173	31.89173	NaN	25	-34.36854	9.41430	-43.78284
7	31.90286	31.90286	NaN	26	-13.36573	30.41942	-43.78515
8	31.88786	31.88786	NaN	27	30.41995	30.41995	NaN
9	25.96631	25.96631	NaN	28	16.41628	16.41628	NaN

10	25.97712	25.97712	NaN	29	16.42316	16.42316	NaN
11	14.66366	14.66366	NaN	30	31.88656	31.88656	NaN
12	14.67724	14.67724	NaN	31	31.88447	31.88447	NaN
13	14.67474	14.67474	NaN	32	31.88789	31.88789	NaN
14	14.67120	14.67120	NaN	33	-11.89461	31.88654	-43.78115
15	30.37445	30.37445	NaN	34	-29.07559	14.68380	-43.75939
16	16.41932	16.41932	NaN	35	14.68819	14.68819	NaN
17	16.42492	16.42492	NaN	36	25.98580	25.98580	NaN
18	16.42575	16.42575	NaN	37	25.98567	25.98567	NaN
19	16.42446	16.42446	NaN	38	27.70656	27.70656	NaN

Note: NaN represents no value.

References

S1. J. A. Letizia, S. Cronin, R. P. Ortiz, A. Facchetti, M. A. Ratner and T. J. Marks, Phenacyl-thiophene and quinone semiconductors designed for solution processability and air-stability in high mobility n-channel field-effect transistors, *Chem. Eur. J.*, 2010, **16**, 1911-1928.

S2. Q. Xing, K. Song, T. Liang, Q. Liu, W. Sun and C. Redshaw, Synthesis, characterization and ethylene polymerization behaviour of binuclear nickel halides bearing 4,5,9,10-tetra(arylimino)pyrenylidenes, *Dalton. Trans.*, 2014, **43**, 7830.

S3. Q. Li, D. N. Li, H. D. Wang, H. G. Wang, Y. H. Li, Z. J. Si, Q. Duan, Conjugated carbonyl polymer-based flexible cathode for superior lithium-organic batteries, *ACS Appl. Mater. Inter.*, 2019, **11**, 28801-28808.

S4. I. Avilov, P. Minoofar, J. M. Cornil and L. De Cola, Influence of substituents on the energy and nature of the lowest excited states of heteroleptic phosphorescent Ir(III) complexes: a joint theoretical and experimental study, *J. Am. Chem. Soc*., 2007, **129**, 8247-8258

S5. J. Burgdörfer and L. J. Dubé, Multiple-scattering approach to coherent excitation in electron-capture collisions, *Phys. Rev. Lett*., 1984, **52**, 2225-2228.

S6. T. Lu and F. Chen, Multiwfn: a multifunctional wavefunction analyzer, *J. Comput. Chem.*, 2012, **33**, 580-592.

S7. W. Humphrey, A. Dalke and K. Schulten, VMD: visual molecular dynamics, *J. Mol. Graph.*, 1996, **14**, 33-38.

S8. N. Zindy, C. Aumaitre, M. Mainville, H. Saneifar, P. A. Johnson, D. Bélanger, and M. Leclerc, Pyrene diimide-based π-conjugated copolymer and single walled carbon nanotube composites for lithium ion batteries, *Chem. Mater.*, 2019, **31**, 8764–8773.

S9. Z. H. Ba, Z. X. Wang, M. Luo, H. B. Li, Y. Z. Li, T. Huang, J. Dong, Q. H. Zhang, and X. Zhao, Benzoquinone-based polyimide derivatives as high-capacity and stable organic cathodes for lithium-ion batteries, *ACS Appl. Mater. Inter.*, 2020, **12**, 807–817.

S10. G. Wang, N. Chandrasekhar, B. P. Biswal, D. Becker, S. Paasch, E. Brunner, M. Addicoat, M. Yu, R. Berger, and X. L. Feng, A Crystalline, 2D Polyarylimide Cathode for Ultrastable and Ultrafast Li Storage, *Adv. Mater.,* 2019, **31**, 1901478.

S11. A. Molina, N. Patil, E. Ventosa, M. Liras, J. Palma and R. Marcilla, New anthraquinone-based conjugated microporous polymer cathode with ultrahigh specific surface area for high-performance lithium-ion batteries, *Adv. Funct. Mater.*, 2020, **30**, 1908074.

S12. X. Y. Han, C. X. Chang, L. J. Yuan, T. L. Sun, and J. T. Sun, Aromatic carbonyl derivative polymers as high-performance li-ion storage materials, *Adv. Mater.*, 2007, **19**, 1616-1621.

S13. C. Y. Chen, X. Zhao, H. B. Li, F. Gan, J. X. Zhang, J. Dong and Q. H. Zhang, Naphthalene-based polyimide derivatives as organic electrode materials for lithium-ion batteries, *Electrochim. Acta*, 2017, **229**, 387-395.

S14. D. Tian, H. Z. Zhang, D. S. Zhang, Z. Chang, J. Han, X. P. Gao and X. H. Bu,

Li-ion storage and gas adsorption properties of porous polyimides (PIs), *RSC Adv.*, 2014, **4**, 7506-7510.

S15. F. Xu, J. T. Xia, W. Shi and S. A. Cao, Sulfonyl-based polyimide cathode for lithium and sodium secondary batteries: enhancing the cycling performance by the electrolyte, *Mater. Chem. Phys.*, 2016, **169**, 192-197.

S16. C. P. Yuan, Q. Wu, Q. Shao, Q. Li, B. Gao, Q. Duan and H. G. Wang, Free-standing and flexible organic cathode based on aromatic carbonyl compound/carbon nanotube composite for lithium and sodium organic batteries, *J. Colloid Interf. Sci.*, 2018, **517**, 72-79.

S17. C. P. Yuan, Q. Wu, Q. Li, Q. Duan, Y. H. Li and H. G. Wang, Nanoengineered ultralight organic cathode based on aromatic carbonyl compound/graphene aerogel for green lithium and sodium ion batteries, *ACS Sustain. Chem. Eng.*, 2018, **6**, 8392-8399.